

Article

# Synthesis of Aligned TiO<sub>2</sub> Nanofibers Using Electrospinning

Jae-Hun Kim, Jae-Hyoung Lee, Jin-Young Kim and Sang Sub Kim \*

Department of Materials Science and Engineering, Inha University, Incheon 22212, Korea; kjhbb5331@gmail.com (J.-H.K.); jhlee5321@naver.com (J.-H.L.); piadote@naver.com (J.-Y.K.)

\* Correspondence: sangsub@inha.ac.kr; Tel.: +82-32-860-7546

Received: 24 January 2018; Accepted: 17 February 2018; Published: 21 February 2018

**Abstract:** In this work, aligned TiO<sub>2</sub> nanofibers (NFs) were synthesized using an electrospinning technique with a two-piece Al collector. The effects of processing parameters, including the calcination temperature, applied voltage, and needle-to-Al-collector distance, were studied. The final phase of TiO<sub>2</sub> was determined using the calcination temperature; calcination at 500 °C resulted in the formation of anatase phase, whereas calcination at 600 °C resulted in the formation of rutile phase. In addition, with the increase of calcination temperature, the diameter of the synthesized NFs decreased owing to the sintering and coalescence of nanograins existing in individual NFs. A specially designed collector configuration resulted in the parallel alignment of TiO<sub>2</sub> NFs. The needle-to-collector distance and applied voltages caused the change in diameter and alignment of NFs. The diameter had an inverse relation with the needle-to-collector distance, and an optimal value of applied voltage was required to achieve TiO<sub>2</sub> NFs with the smallest diameter. Furthermore, with the increase of applied voltage, the morphology of TiO<sub>2</sub> NFs changed from an aligned to a disordered state.

**Keywords:** aligned TiO<sub>2</sub>; nanofiber; process parameters; electrospinning

## 1. Introduction

Titanium dioxide (TiO<sub>2</sub>) is one of the most important functional materials with promising electronic and optical properties. It has a band gap of ~3.2 eV for anatase and brookite phases and ~3.0 eV for rutile phase, with n-type semiconducting properties [1]. Additionally, TiO<sub>2</sub> is transparent and has a high refractive index [2]. Accordingly, it is extensively used for different applications such as gas sensing [3], fuel cells [4], photocatalysis [5,6], photovoltaics [7,8], and photonics [9]. Owing to the high surface-to-volume ratio of one-dimensional (1-D) nanomaterials, TiO<sub>2</sub> nanostructures with 1-D morphology such as nanorods [10], nanowires [11], nanotubes [12], and nanofibers (NFs) [13] are generally utilized for applications requiring a high surface-to-volume ratio, resulting in the enhanced performance of the fabricated device. However, most applications require the size of TiO<sub>2</sub> to be controllable for better performance, which is not easily realized.

Among the aforementioned morphologies, NFs have the advantage of easy synthesis using the cost-effective and facile electrospinning (ES) method [14]. By using the ES method, the diameter of the synthesized NFs can be adjusted by controlling the processing variables [15]. In a typical process of ES, under the effect of an electric field, a viscous solution is extruded from a needle to form a small droplet. If the electric field is sufficiently large, a liquid jet is formed and it accelerates toward a grounded conductive collector, which is at a given distance from the needle, and thus NFs can be produced [16]. The NFs are often deposited without preferred alignment. The morphology and diameter of the synthesized NFs are affected by the intrinsic properties of the solution and operational conditions such as the strength of the applied field and needle-to-collector distance. By controlling these variables, it is possible to control the diameter, length, and alignment of the synthesized NFs [17].

Well-aligned and highly ordered NFs can lead to a higher molecular orientation and degree of crystallinity and, as a result, better mechanical properties [18]. Furthermore, due to the existence of a long 1-D current path, the electrons can flow faster within aligned NFs relative to non-aligned NFs, where there are more junctions among NFs. Therefore, aligned NFs have enhanced electronic transport properties. [19].

Accordingly, the alignment of NFs is important for various applications. For example, microelectronics and photonics devices often require well-aligned and highly ordered structures to demonstrate their best performances [18]. Field-emission sources with highly aligned architectures are highly efficient [20]. Nanosensors with an aligned structure can offer better sensitivity [21]. Optical properties of devices with an aligned structure can be enhanced [22]. In tissue engineering, aligned NFs significantly enhance cell response [23].

Accordingly, many researchers have investigated different strategies to control the parameters of ES in order to obtain aligned NFs [24–26]. A simple method to generate uniaxially aligned NFs is to introduce a small gap into a charged collector [16]. The as-spun NFs produced via normal ES are highly charged. As the bending instability of a charged jet initiates its movement, as-electrospun NFs are generally randomized. Further, in the presence of a single grounded conductive plate used as the collector, electrostatic forces (strong external field, collector, and any adjacent charged NFs) affect the motion of the ejected fiber and there is no preferential direction of the as-spun NFs in the collector. Consequently, NFs are randomly collected on the surface of the collector. In contrast, when an insulating gap (air) is introduced into the conductive collector, the configuration of the electric field is changed. Thus, the directions of the electrostatic forces acting on the NFs are changed, which can eventually change the forces acting on the fiber and consequently the alignment of NFs [18].

In this study, we synthesized aligned TiO<sub>2</sub> using the ES method with polyvinyl pyrrolidone (PVP) and Ti tetraisopropoxide (Ti(OiPr)<sub>4</sub>) as precursors. We studied the effects of changing the calcination temperature, applied voltage, and needle-to-Al-collector distance on the final diameter of the synthesized TiO<sub>2</sub> NFs. It was observed that all of the studied parameters affected the final diameters and alignment of the synthesized NFs. Therefore, this work highlights the need for the optimization of the process parameters to achieve aligned TiO<sub>2</sub> NFs with small diameters.

## 2. Materials and Methods

### 2.1. Synthesis of Viscous Solution of PVP and (Ti(OiPr)<sub>4</sub>)

In order to synthesize TiO<sub>2</sub> NFs using ES, PVP (Mw 1,300,000 g·mol<sup>-1</sup>) and Ti tetraisopropoxide (Ti(OiPr)<sub>4</sub>) were used as the starting materials. First, a solvent composed of acetic acid (27 wt.%) and ethanol (73 wt.%) was prepared. A mixed solvent was also used in other studies [27,28]. Ethanol was chosen due to the easy evaporation during the electrospinning process and acetic acid was chosen due to the increase of solution viscosity and dissolution of precursors. Subsequently, a PVP solution was prepared by dissolving 7.5 wt.% PVP in a mixed solvent while stirring for 4 h at 75 °C. Then, 10 wt.% (Ti(OiPr)<sub>4</sub>) was added to the PVP solution under magnetic stirring at 75 °C for 6 h until a homogeneous viscous solution containing PVP and (Ti(OiPr)<sub>4</sub>) was obtained.

### 2.2. ES Procedure

In this study, a special ES apparatus was used to synthesize well-aligned TiO<sub>2</sub> NFs. Usually, a collector is used in the ES process, but in this study, two Al collectors were used and grounded with a negative charge. The distance between the two collectors was 2 cm. Figure 1 shows the schematic illustration of the ES apparatus. The prepared viscous solution of PVP and (Ti(OiPr)<sub>4</sub>) was drawn into a syringe with a 21-gauge stainless steel needle. The distance between the tip of the needle and the two-piece collector was varied from 20 to 40 cm. A positive high voltage of +10 kV was applied to the needle, whereas a negative voltage (from -5 to -20 kV) was applied to the collector to accelerate the ES process. The feeding rate during the ES process was set to be 0.05 mL/h using a syringe pump.

Electrospun TiO<sub>2</sub> NFs were distributed onto the Al collector and thereafter calcined in air at 500 and 600 °C for 6 h to obtain crystalline TiO<sub>2</sub> NFs.

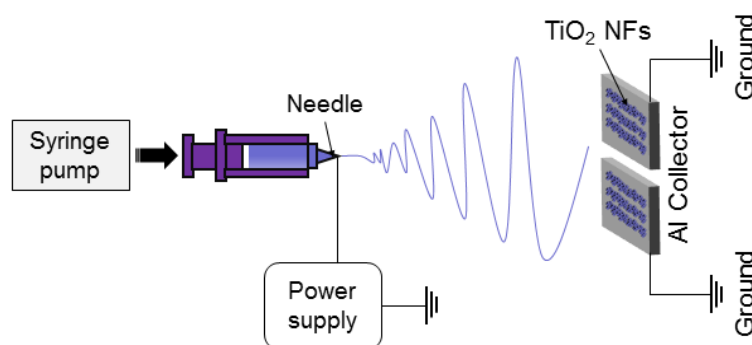


**Figure 1.** Schematic illustration of electrospinning (ES) apparatus.

### 2.3. Characterizations

The morphology of the synthesized NFs was studied using field-emission scanning electron microscopy (FE-SEM- Hitachi S-4200) operating with a 20-kV accelerating voltage. X-ray diffraction patterns (XRD, Philips Xpert MRD diffractometer) were recorded at room temperature at a scan rate of 0.5 °/min using Cu K<sub>α</sub> ( $\lambda = 1.5406 \text{ \AA}$ ) radiation. XRD was used to examine the crystallinity and phase formation of the synthesized TiO<sub>2</sub> NFs.

### 3. Results and Discussion

TiO<sub>2</sub> is a polymorphous material and has three crystalline phases, namely anatase, brookite, and rutile [29]. Rutile is the most stable polymorph, but anatase and brookite are also common [30]. Therefore, XRD was used to analyze the crystallinity of the synthesized TiO<sub>2</sub> NFs and to determine the formed phase. It should be noted that the choice of calcination temperature was based on our previous study [15], where using thermogravimetric analysis (TGA), differential thermal analysis (DTA) and XRD experiments we showed that calcinations at 500 and 600 °C resulted in the formation of different TiO<sub>2</sub> phases. Furthermore, other researchers have reported the calcination of TiO<sub>2</sub> NFs at 500 °C [28,31], and 600 °C [32]. In the initial stages of ES, Ti(OiPr)<sub>4</sub> is hydrolyzed by reacting with moisture in the air to form ultrafine particles of amorphous TiO<sub>2</sub> in the PVP matrix. Accordingly, the as-spun NFs do not show any crystallinity [33]. However, amorphous TiO<sub>2</sub> can be crystallized by calcination at a high temperature. Figure 2a shows the XRD pattern of TiO<sub>2</sub> NFs calcined at 500 °C for 6 h. It shows peaks centered at 25.5, 37.9, 49.1, 55.2, 63.2, 68.8, and 76.2° corresponding to the (101), (002), (200), (211), (204), (116), and (101) planes of TiO<sub>2</sub> with tetragonal anatase phase (JCPDS No. 21-1272), respectively. The broadening of the diffraction peaks is due to the very small size of the TiO<sub>2</sub> nanocrystals [33]. In the literature, it is reported that anatase can be crystallized as the first crystalline phase from amorphous TiO<sub>2</sub>. From a thermodynamic point of view, anatase is the phase with the lowest total energy, and a lower surface energy accelerates the nucleation kinetics and facilitates the formation of anatase [34].

Representative XRD patterns of TiO<sub>2</sub> calcined NFs at 600 °C and 500 °C and as-spun TiO<sub>2</sub> NFs are shown in Figure 2. It shows peaks located at 27.5, 36.2, 41.3, 54.4, 56.7, and 69.2°, which can be attributed to the (110), (101), (111), (211), (220), and (301) planes of TiO<sub>2</sub> with rutile structure, respectively, which is consistent with the literature [35]. Thus, by controlling the calcination temperature from 500 to 600 °C, it is possible to obtain crystalline phases with anatase (at 500 °C) or rutile structures (at 600 °C).

Figure 3a,b show the FE-SEM images of the as-spun NFs at different magnifications. It is evident that long and continuous NFs were formed. From the high-magnification FE-SEM image, the diameter of the as-spun NFs without calcination was estimated to be 720 nm. The large diameter of the as-spun NFs is mainly due to the existence of water and the PVP matrix. Figure 3c,d show the FE-SEM images of NFs crystallized at 500 °C for 6 h. It is evident that the NFs retained their morphology after calcination

and, from the high-magnification image, the diameter of NFs calcined at 500 °C was estimated to be 150 nm. Therefore, the diameter decreased significantly in comparison with the as-spun NFs. This is due to the evaporation of the solvent and PVP molecules at high temperatures. From a comparison between the high-magnification images of the as-spun NFs (Figure 3b) and NFs calcined at 500 °C, it can be observed that a change of surface morphology occurred from smooth to grainy, owing to the evaporation of the solvent and polymer molecules from the surfaces; consequently, a grainy structure remained on the surface of TiO<sub>2</sub> NFs calcined at 500 °C. Other studies have also reported the formation of a grainy structure of NFs after calcination [36,37]. With the increase of calcination temperature to 600 °C, the sintering and coalescence of nanograins in individual NFs became more evident and, consequently, the diameter of NFs decreased to 130 nm as shown in the FE-SEM images of Figure 3e,f with different magnifications. As shown schematically in Figure 4, before calcination, TiO<sub>2</sub> NFs were amorphous with smooth surfaces without any grains. During the calcination, the diameter significantly decreased because of the evaporation of the polymer species and solvents as well as the decomposition of precursors. Simultaneously, nanosized grains started to grow. With the increase of calcination temperature, the nanograins coalesced with each other owing to the increase of diffusion rate, resulting in a significantly larger growth of nanograins and smaller fiber diameter [38,39].

In the literature, many researchers have reported the effect of applied potential on the final morphology or diameter of synthesized NFs [40–42]. If the applied potential is lower than a threshold value, no stable liquid jets will be formed [43]. Once a threshold voltage is exceeded, a stable jet of liquid is directed toward the collector. We changed the applied potential by maintaining the positive voltage constant at +10 V and changing the negative voltage (−5, −10, and −20 V). As shown in Figure 5, with the increase of applied potential, the diameter first decreased and thereafter increased. As shown in Figure 5a,b, by applying the voltages of +10 and −5 V, the final diameter of TiO<sub>2</sub> NFs after calcination at 600 °C was 200 nm, and with the increase of negative voltage to −10 V, it decreased to 130 nm (Figure 5c,d); moreover, with the further increase of negative voltage to −20 V (Figure 5e,f), the final diameter increased to 195 nm.

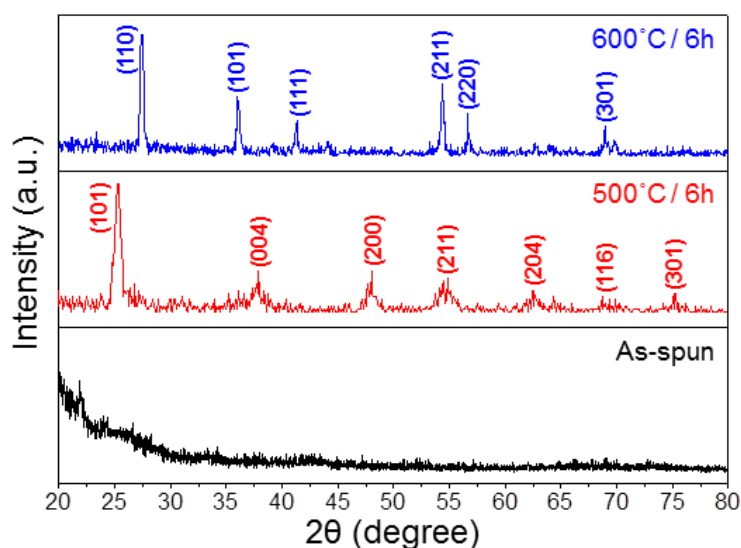


**Figure 2.** X-ray diffraction (XRD) patterns of TiO<sub>2</sub> nanofibers (NFs) calcined at 500 °C for 6 h and 600 °C for 6 h, and as-spun TiO<sub>2</sub> NFs.

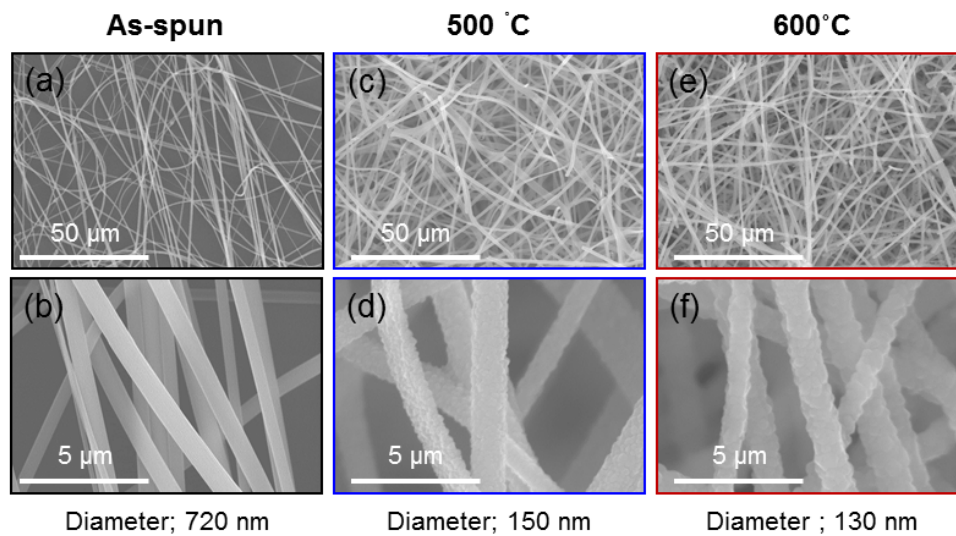


**Figure 3.** Low- and high-magnification FE-SEM images of synthesized TiO<sub>2</sub> NFs. (a,b) As-spun NFs; (c,d) NFs calcined at 500 °C for 6 h; (e,f) NFs calcined at 600 °C for 6 h.

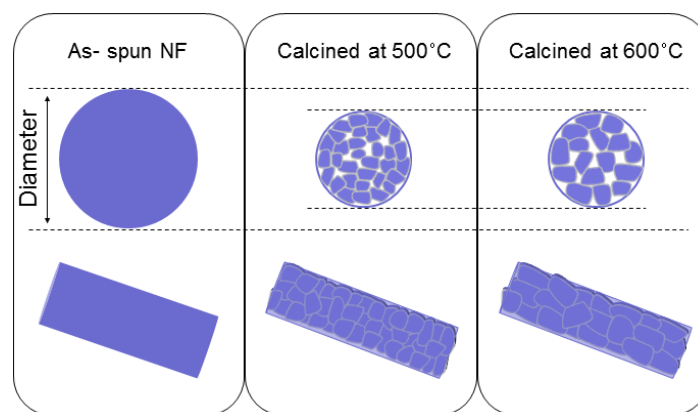


**Figure 4.** Schematic illustration of the growth of nanograins in NFs with the increase of calcination temperature (modified from Reference [33]).

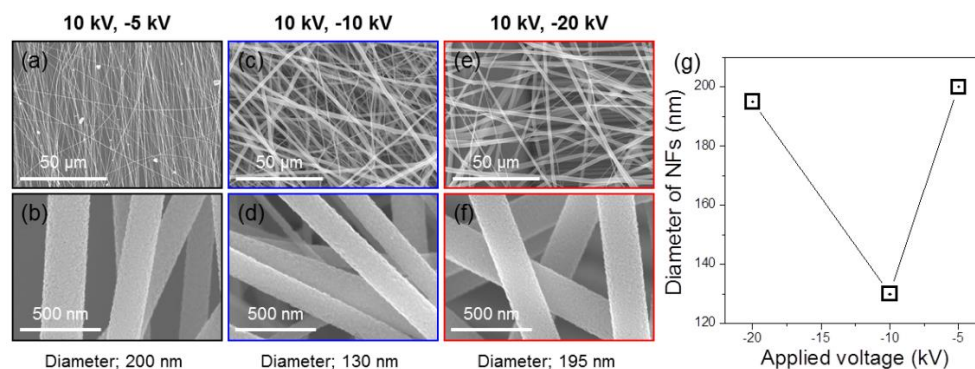


**Figure 5.** Low- and high-magnification FE-SEM images of synthesized TiO<sub>2</sub> NFs prepared with different applied voltages: (a,b) 10 and −5 kV; (c,d) 10 and −10 kV; (e,f) 10 and −20 kV; (g) Diameter of obtained TiO<sub>2</sub> NFs as a function of applied voltage.

Figure 5g shows the relationship between the diameters of TiO<sub>2</sub> NFs and applied voltage. To explain the changes of diameter with the change of applied voltage, the following forces acting on

a charged jet should be considered [44]: (i) gravitational force; (ii) electrostatic force responsible for the acceleration of the formed jet to the collector; (iii) Coulombic force stretching the jet; (iv) viscoelastic force; (v) surface tension (both viscoelastic force and surface tension prevent the stretching of the charged jet); and (vi) drag force owing to the friction between the charged jet and the surrounding atmosphere. The effect of applied potential on the diameters of NFs can be determined using the relationships among the Coulombic and viscoelastic forces and surface tension. At low applied potentials ( $-5$  kV), the Coulombic force is smaller than the viscoelastic and surface tension. Consequently, NFs with large diameters are formed. At moderate applied potentials ( $-10$  kV), all three forces are balanced, resulting in the decrease of diameters of NFs. With a further increase in the applied potentials ( $-20$  kV), the Coulombic force becomes much greater than the viscoelastic force and surface tension. However, as there is both longitudinal and transverse stretching and the latter can lead to the increase of diameter of NFs, the increased diameter of NFs obtained in this study can be attributed to the dominance of transverse stretching relative to longitudinal stretching. Furthermore, with the increase of applied potential, the formed jet can accelerate faster toward the collector; thus, the solvent would not have sufficient time to evaporate, eventually leading to the formation of NFs with a larger diameter [44]. It should be noted that by comparing between Figure 5a,c,e, it can be seen that under the lowest applied voltage, some beads appear. This may be due to the fact that the low applied voltage leads to the viscoelastic force which can lead to the formation of some beads.

It can be observed that the  $\text{TiO}_2$  NFs produced at the lowest applied voltage ( $-5$  kV) were aligned, whereas with the increase of voltage, disordered  $\text{TiO}_2$  NFs were obtained. As schematically shown in Figure 6, the as-spun charged NFs can be aligned if they are affected by pulling forces. Electrostatic forces pull the two ends of the NFs toward the two collectors and consequently align the NFs. Under the effect of pulling forces, the NFs turn perpendicularly toward the edges of the collectors. Subsequently, the two ends of the NFs are deposited on the collectors. If these steps are repeated, arrays of uniaxially aligned NFs can be obtained across the gap [18].

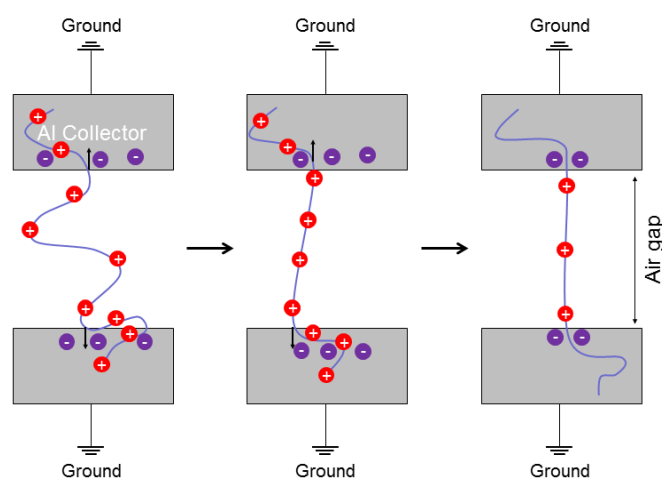


**Figure 6.** Schematic illustration of the process of alignment of NFs (modified from Reference [25]).

The effects of voltage can be ascribed to the “whipping” instability. During ES, the rapid growth of a nonaxisymmetric or whipping instability resulted in the bending of NFs and permitted the electrical forces to elongate the jet. With the increase of the applied voltage, whipping instability increased accordingly, leading to the entanglement and knotting of the as-spun NFs and rendered the alignment of NFs more difficult. Hence, the alignment of NFs is not possible at high applied voltages [18].

In the subsequent step, while the positive and negative voltages were fixed at  $+15$  and  $-10$  kV, respectively, the distance between the needle and Al collector was changed (20, 30, and 40 cm). Figure 7a,b show the low- and high-magnification FE-SEM micrographs of  $\text{TiO}_2$  NFs with the

needle-to-Al-collector distance of 20 cm after calcination at 600 °C, respectively. The synthesized NFs were long and continuous with an approximate diameter of 150 nm. With the increase of needle-to-Al-collector distance to 30 cm, as shown in Figure 7c,d, the diameter increased to 185 nm, and with the further increase of needle-to-Al-collector distance to 40 cm, the diameter increased to 245 nm (Figure 7e,f). It is expected that, with the increase of needle-to-collector distance, the solvent has more time to evaporate; therefore, a smaller diameter should be obtained [45]. However, the experimental results exhibit a contrasting trend, as shown in Figure 7g. With the increase of needle-to-collector distance, the strength of the electric field, defined as the applied voltage divided by the distance between the needle and collector, decreased. Thus, it can be concluded that, with the decrease of electric field, the viscoelastic force increased, which prevented the stretching of NFs, resulting in the increase of the diameter of NFs. From Figure 7a, c, and e, it can be seen that at a short distance, some beads appear. This is likely due to the fact that the electrospinning solution reaches the Al collector before the full evaporation of the solvent [45].

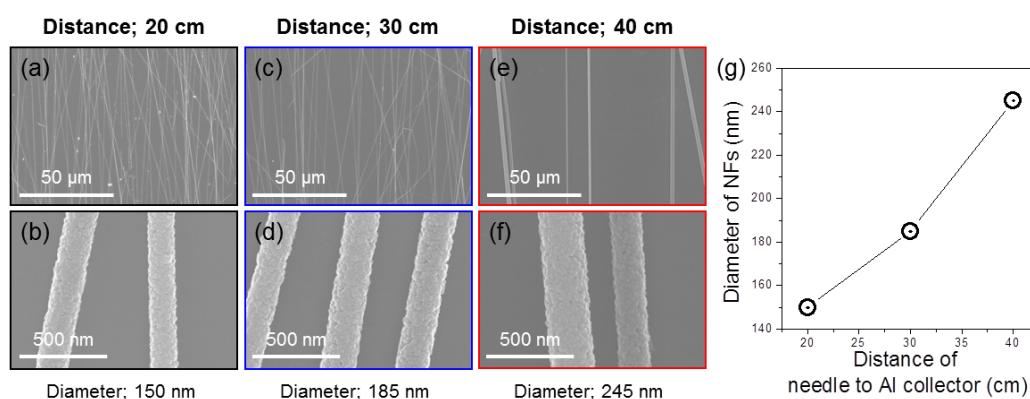


**Figure 7.** Low- and high-magnification FE-SEM images of synthesized TiO<sub>2</sub> NFs prepared with different distances between the needle and Al collector: (a,b) 20 cm; (c,d) 30 cm; (e,f) 40 cm; (g) Diameter of obtained TiO<sub>2</sub> NFs as a function of needle-to-collector distance.

From Figures 5 and 7, it may be noticed that with the increase of either applied voltage or needle-to-Al-collector distance, the number of the produced NFs was decreased. This can be explained partly the fact that if the distance is long, some formed NFs may be unable to reach to the Al collector. However, more works should be carried out to clarify the reason behind the phenomena that occur with the increase of applied voltages.

As shown in Figure 7, the alignment of NFs did not change significantly with the increase of needle-to-collector distance. As stated before, with the increase of needle-to-collector distance, the electric field acting on the NFs decreased, and consequently, whipping instability, which is responsible for bending and allows the electrical forces to elongate the jet, decreased. Therefore, the as-spun NFs did not lose their aligned morphology with the increase of needle-to-collector distance. For the nanoscale applications, where the diameter of TiO<sub>2</sub> NFs directly affects the device performance, the difference observed among the synthesized TiO<sub>2</sub> NFs in this study can be significant. In this study, the air gap distance between the two Al collectors was remained constant. However, the change in the air gap distance can greatly influence the morphology and alignment of NFs [16,18].

#### 4. Conclusions

In summary, aligned TiO<sub>2</sub> NFs were synthesized using a special ES method with a two-piece Al collector. The effect of various variables, i.e., calcination temperature, applied potential, and needle-to-collector distance, on the final crystalline phase, diameter, and alignment of the formed TiO<sub>2</sub> NFs were investigated. It was revealed that the calcination temperature influences the diameter and

final phase of the crystallized NFs. Moreover, the distance between the needle and collector and the applied voltage influence the final diameter and alignment of TiO<sub>2</sub> NFs. This study demonstrated that, by controlling the needle-to-collector distance and applied voltage, well-aligned TiO<sub>2</sub> NFs with controllable diameters can be obtained.

**Acknowledgments:** This study was supported by Inha University.

**Author Contributions:** Sang Sub Kim conceived and designed the experiments and completed the paper; Jin-Young Kim and Jae-Hyoung Lee performed the experiments; Jae-Hun Kim analyzed the data and prepared the draft of the paper.

**Conflicts of Interest:** The authors declare no conflict of interest and the founding sponsors had no role in the design of the study; in the collection, analyses, or interpretation of data; in the writing of the manuscript, and in the decision to publish the results.

## References

1. Kumar, S.G.; Devi, L.G. Review on Modified TiO<sub>2</sub> Photocatalysis under UV/Visible Light: Selected Results and Related Mechanisms on Interfacial Charge Carrier Transfer Dynamics. *J. Phys. Chem. A* **2011**, *115*, 13211–13241. [[CrossRef](#)] [[PubMed](#)]
2. Watthanaarun, J.; Pavarajarn, V.; Supaphol, P. Titanium (IV) Oxide Nanofibers by Combined Sol–Gel and Electrospinning Techniques: Preliminary Report on Effects of Preparation Conditions and Secondary Metal Dopant. *Sci. Technol. Adv. Mater.* **2005**, *6*, 240–245. [[CrossRef](#)]
3. Park, J.Y.; Choi, S.-W.; Lee, J.-W.; Lee, C.; Kim, S.S. Synthesis and Gas Sensing Properties of TiO<sub>2</sub>–ZnO Core-Shell Nanofibers. *J. Am. Ceram. Soc.* **2009**, *92*, 2551–2554. [[CrossRef](#)]
4. Drew, K.; Girishkumar, G.; Vinodgopal, K.; Kamat, P.V. Boosting Fuel Cell Performance with a Semiconductor Photocatalyst: TiO<sub>2</sub>/Pt–Ru Hybrid Catalyst for Methanol Oxidation. *J. Phys. Chem. B* **2005**, *109*, 11851–11857. [[CrossRef](#)] [[PubMed](#)]
5. Ni, M.; Leung, M.K.H.; Leung, D.Y.C.; Sumathy, K. A Review and Recent Developments in Photocatalytic Water-Splitting Using TiO<sub>2</sub> for Hydrogen Production. *Renew. Sustain. Energ. Rev.* **2007**, *11*, 401–425. [[CrossRef](#)]
6. Daghri, R.; Drogui, P.; Robert, D. Modified TiO<sub>2</sub> for Environmental Photocatalytic Applications: A Review. *Ind. Eng. Chem. Res.* **2013**, *52*, 3581–3599. [[CrossRef](#)]
7. Kim, Y.-G.; Walker, J.; Samuelson, L.A.; Kumar, J. Efficient Light Harvesting Polymers for Nanocrystalline TiO<sub>2</sub> Photovoltaic Cells. *Nano Lett.* **2003**, *3*, 523–525. [[CrossRef](#)]
8. Koo, H.J.; Kim, Y.J.; Lee, Y.H.; Lee, W.I.; Kim, K.; Park, N.G. Nano-Embossed Hollow Spherical TiO<sub>2</sub> as Bifunctional Material for High-Efficiency Dye-Sensitized Solar Cells. *Adv. Mater.* **2008**, *20*, 195–199. [[CrossRef](#)]
9. Lu, Y.; Yu, H.; Chen, S.; Quan, X.; Zhao, H. Integrating Plasmonic Nanoparticles with TiO<sub>2</sub> Photonic Crystal for Enhancement of Visible-Light-Driven Photocatalysis. *Environ. Sci. Technol.* **2012**, *46*, 1724–1730. [[CrossRef](#)] [[PubMed](#)]
10. Liu, B.; Aydil, E.S. Growth of Oriented Single-Crystalline Rutile TiO<sub>2</sub> Nanorods on Transparent Conducting Substrates for Dye-Sensitized Solar Cells. *J. Am. Chem. Soc.* **2009**, *131*, 3985–3990. [[CrossRef](#)] [[PubMed](#)]
11. Armstrong, A.R.; Armstrong, G.; Canales, J.; García, R.; Bruce, P.G. Lithium-Ion Intercalation into TiO<sub>2</sub>-B Nanowires. *Adv. Mater.* **2005**, *17*, 862–865. [[CrossRef](#)]
12. Zhu, K.; Neale, N.R.; Miedaner, A.; Frank, A.J. Enhanced Charge-Collection Efficiencies and Light Scattering in Dye-Sensitized Solar Cells Using Oriented TiO<sub>2</sub> Nanotubes Arrays. *Nano Lett.* **2007**, *7*, 69–74. [[CrossRef](#)] [[PubMed](#)]
13. Kim, I.-D.; Rothschild, A.; Lee, B.H.; Kim, D.Y.; Jo, S.M.; Tuller, H.L. Ultrasensitive Chemiresistors Based on Electrospun TiO<sub>2</sub> Nanofibers. *Nano Lett.* **2006**, *6*, 2009–2013. [[CrossRef](#)] [[PubMed](#)]
14. Formo, E.; Lee, E.; Campbell, D.; Xia, Y. Functionalization of Electrospun TiO<sub>2</sub> Nanofibers with Pt Nanoparticles and Nanowires for Catalytic Applications. *Nano Lett.* **2008**, *8*, 668–672. [[CrossRef](#)] [[PubMed](#)]
15. Park, J.Y.; Kim, S.S. Effects of Processing Parameters on the Synthesis of TiO<sub>2</sub> Nanofibers by Electrospinning. *Met. Mater. Int.* **2009**, *15*, 95–99. [[CrossRef](#)]
16. Li, D.; Wang, Y.; Xia, Y. Electrospinning of Polymeric and Ceramic Nanofibers as Uniaxially Aligned Arrays. *Nano Lett.* **2003**, *3*, 1167–1171. [[CrossRef](#)]
17. Li, D.; Xia, Y. Electrospinning of Nanofibers: Reinventing the Wheel? *Adv. Mater.* **2004**, *16*, 1151–1170. [[CrossRef](#)]

18. Jalili, R.; Morshed, M.; Ravandi, S.A.H. Fundamental Parameters Affecting Electrospinning of PAN Nanofibers as Uniaxially Aligned Fibers. *J. Appl. Polym. Sci.* **2006**, *101*, 4350–4357. [[CrossRef](#)]
19. Choi, S.-H.; Ankonina, G.; Youn, D.Y.; Oh, S.G.; Hong, J.M.; Rothschild, A.; Kim, I.D. Hollow ZnO Nanofibers Fabricated Using Electrospun Polymer Templates and Their Electronic Transport Properties. *ACS Nano* **2009**, *3*, 2623–2631. [[CrossRef](#)] [[PubMed](#)]
20. Kovtyukhova, N.I.; Mallouk, T.E. Nanowires as Building Blocks for Self-Assembling Logic and Memory Circuits. *Chem. Eur. J.* **2002**, *8*, 4354–4363. [[CrossRef](#)]
21. Teo, K.; Chhowalla, M.; Amaratunga, G.; Milne, W.; Pirio, G.; Legagneux, P.; Wyczisk, F.; Pribat, D.; Hasko, D. Field Emission from Dense, Sparse, and Patterned Arrays of Carbon Nanofibers. *Appl. Phys. Lett.* **2002**, *80*, 2011–2013. [[CrossRef](#)]
22. Zhu, Z.; Zhang, L.; Howe, J.Y.; Liao, Y.; Speidel, J.T.; Smith, S.; Fong, H. Aligned Electrospun ZnO Nanofibers for Simple and Sensitive Ultraviolet Nanosensors. *Chem. Commun.* **2009**, *0*, 2568–2570. [[CrossRef](#)] [[PubMed](#)]
23. Yin, K.; Zhang, L.; Lai, C.; Zhong, L.; Smith, S.; Fong, H.; Zhu, Z. Photoluminescence Anisotropy of Uni-Axially Aligned Electrospun Conjugated Polymer Nanofibers of MEH-PPV and P3HT. *J. Mater. Chem.* **2011**, *21*, 444–448. [[CrossRef](#)]
24. Lin, V.S.; Lee, M.C.; O’Neal, S.; McKean, J.; Sung, K.P. Ligament Tissue Engineering Using Synthetic Biodegradable Fiber Scaffolds. *Tissue Eng.* **1999**, *5*, 443–451. [[CrossRef](#)] [[PubMed](#)]
25. Bazbouz, M.B.; Stylios, G.K. Alignment and Optimization of Nylon 6 Nanofibers by Electrospinning. *J. Appl. Polym. Sci.* **2008**, *107*, 3023–3032. [[CrossRef](#)]
26. Theron, A.; Zussman, E.; Yarin, A.L. Electrostatic Field-Assisted Alignment of Electrospun Nanofibres. *Nanotechnology* **2001**, *12*, 384. [[CrossRef](#)]
27. Zhang, X.; Ge, X.; Wang, C. Synthesis of Titania in Ethanol/Acetic Acid Mixture Solvents: Phase and Morphology Variations. *Cryst. Growth Des.* **2009**, *9*, 4301–4307. [[CrossRef](#)]
28. Cheng, Y.; Huang, W.; Zhang, Y.; Zhu, L.; Liu, Y.; Fan, X.; Cao, X. Preparation of TiO<sub>2</sub> Hollow Nanofibers by Electrospinning Combined with Sol-Gel Process. *Cryst. Eng. Commun.* **2010**, *12*, 2256–2260. [[CrossRef](#)]
29. Arbiol, J.; Cerdà, J.; Dezanneau, G.; Cirera, A.; Peiró, F.; Cornet, A.; Morante, J.R. Effects of Nb Doping on the TiO<sub>2</sub> Anatase-to-Rutile Phase Transition. *J. Appl. Phys.* **2002**, *92*, 853–861. [[CrossRef](#)]
30. Vittadini, A.; Casarin, M.; Selloni, A. Chemistry of and on TiO<sub>2</sub>-Anatase Surfaces by DFT Calculations: A Partial Review. *Theor. Chem. Acc.* **2007**, *117*, 663–671. [[CrossRef](#)]
31. Fujihara, K.; Kumar, A.; Jose, R.; Ramakrishna, S.; Uchida, S. Spray Deposition of Electrospun TiO<sub>2</sub> Nanorods for Dye-Sensitized Solar Cell. *Nanotechnology* **2007**, *18*, 365709. [[CrossRef](#)]
32. Park, J.Y.; Choi, S.W.; Asokan, K.; Kim, S.S. Growth of Nanograins in TiO<sub>2</sub> Nanofibers Synthesized by Electrospinning. *J. Nanosci. Nanotechnol.* **2010**, *10*, 3604–3608. [[CrossRef](#)] [[PubMed](#)]
33. Dai, Y.; Cobley, C.M.; Zeng, J.; Sun, Y.; Xia, Y. Synthesis of Anatase TiO<sub>2</sub> Nanocrystals with Exposed {001} Facets. *Nano Lett.* **2009**, *9*, 2455–2459. [[CrossRef](#)] [[PubMed](#)]
34. Reyes-Coronado, D.; Rodríguez-Gattorno, G.; Espinosa-Pesqueira, M.E.; Cab, C.; Coss, R.D.; Oskam, G. Phase-Pure TiO<sub>2</sub> Nanoparticles: Anatase, Brookite and Rutile. *Nanotechnology* **2008**, *19*, 145605. [[CrossRef](#)] [[PubMed](#)]
35. Wang, D.; Choi, D.; Yang, Z.; Viswanathan, V.V.; Nie, Z.; Wang, C.; Song, Y.; Zhang, J.-G.; Liu, J. Synthesis and Li-Ion Insertion Properties of Highly Crystalline Mesoporous Rutile TiO<sub>2</sub>. *Chem. Mater.* **2008**, *20*, 3435–3442. [[CrossRef](#)]
36. Li, Z.; Zhang, H.; Zheng, W.; Wang, W.; Huang, H.; Wang, C.; MacDiarmid, A.G.; Wei, Y. Highly Sensitive and Stable Humidity Nanosensors Based on LiCl Doped TiO<sub>2</sub> Electrospun Nanofibers. *J. Am. Chem. Soc.* **2008**, *130*, 5036–5037. [[CrossRef](#)] [[PubMed](#)]
37. Katsuhiko, O.; Bin, D.; Yosuke, T.; Takayuki, N.; Michiyo, Y.; Shinichiro, S.; Shingo, O.; Masato, Y.; Seimei, S. Electrospinning Processed Nanofibrous TiO<sub>2</sub> Membranes for Photovoltaic Applications. *Nanotechnology* **2006**, *17*, 1026.
38. Park, J.Y.; Choi, S.-W.; Asokan, K.; Kim, S.S. Controlling the Size of Nanograins in TiO<sub>2</sub> nanofibers. *Met. Mater. Int.* **2010**, *16*, 785–788. [[CrossRef](#)]
39. Katoch, A.; Choi, S.-W.; Kim, S.S. Nanograins in Electrospun Oxide Nanofibers. *Met. Mater. Int.* **2015**, *21*, 213–221. [[CrossRef](#)]
40. Deitzel, J.M.; Kleinmeyer, J.; Harris, D.; Beck Tan, N.C. The Effect of Processing Variables on the Morphology of Electrospun Nanofibers and Textiles. *Polymer* **2001**, *42*, 261–272. [[CrossRef](#)]

41. Jarusuwannapoom, T.; Hongrojjanawiwat, W.; Jitjaicham, S.; Wannatong, L.; Nithitanakul, M.; Pattamaprom, C.; Koombhongse, P.; Rangkupan, R.; Supaphol, P. Effect of Solvents on Electro-Spinnability of Polystyrene Solutions and Morphological Appearance of Resulting Electrospun Polystyrene Fibers. *Eur. Polym. J.* **2005**, *41*, 409–421. [[CrossRef](#)]
42. Sukigara, S.; Gandhi, M.; Ayutsede, J.; Micklus, M.; Ko, F. Regeneration of Bombyx Mori Silk by Electrospinning-Part 1: Processing Parameters and Geometric Properties. *Polymer* **2003**, *44*, 5721–5727. [[CrossRef](#)]
43. Li, D.; Xia, Y. Fabrication of Titania Nanofibers by Electrospinning. *Nano Lett.* **2003**, *3*, 555–560. [[CrossRef](#)]
44. Wannatong, L.; Sirivat, A.; Supaphol, P. Effects of Solvents on Electrospun Polymeric Fibers: Preliminary Study on Polystyrene. *Polym. Int.* **2004**, *53*, 1851–1859. [[CrossRef](#)]
45. Chowdhury, M.; Stylios, G. Effect of Experimental Parameters on the Morphology of Electrospun Nylon 6 Fibres. *Int. J. Basic Appl. Sci.* **2010**, *10*, 70–78.



© 2018 by the authors. Licensee MDPI, Basel, Switzerland. This article is an open access article distributed under the terms and conditions of the Creative Commons Attribution (CC BY) license (<http://creativecommons.org/licenses/by/4.0/>).